

Supporting Information

Tuning photoionization mechanisms of hybrid molecular materials for EUV lithography applications

Lianjia Wu,^a Martijn Tiekkink,^a Alexandre Giuliani,^b Laurent Nahon^b and Sonia Castellanos*^a

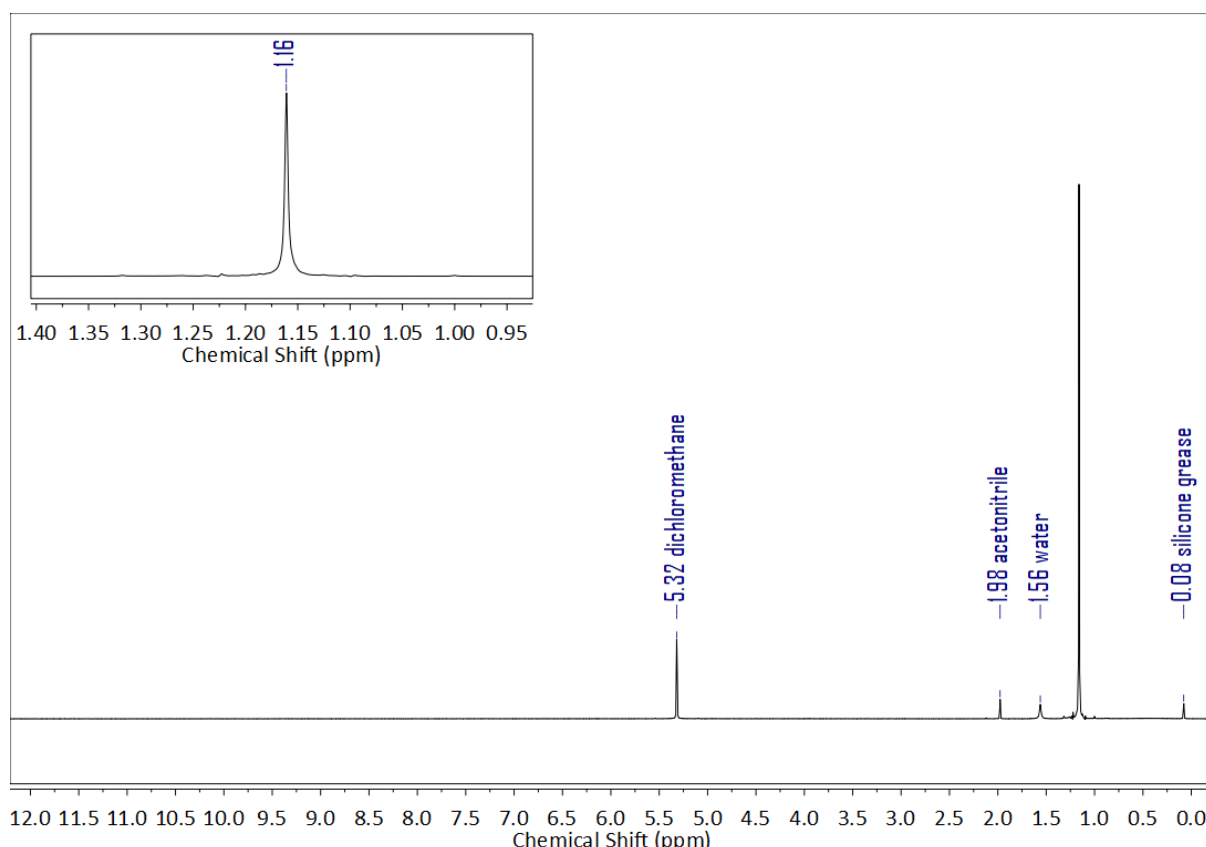


Figure S1. ^1H NMR spectrum of $\text{Ti}_8\text{O}_8(\text{OOC}^{\text{t}}\text{Bu})_{16}$ (Ti_8L_{16}) in CD_2Cl_2 .

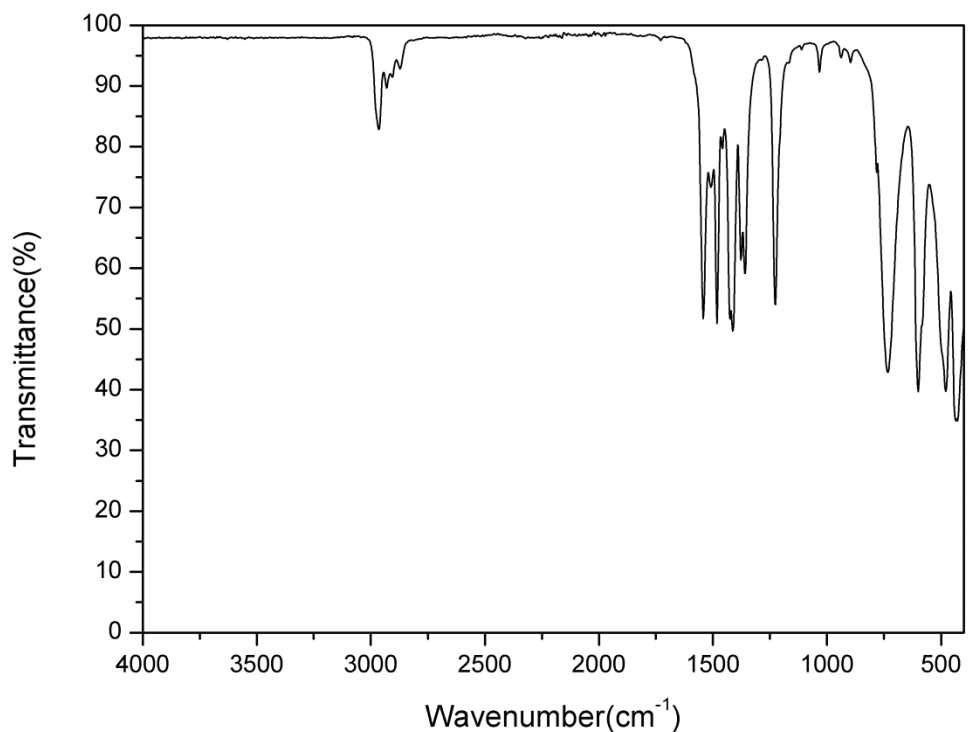


Figure S2. ATR-IR spectrum of Ti_8L_{16} .

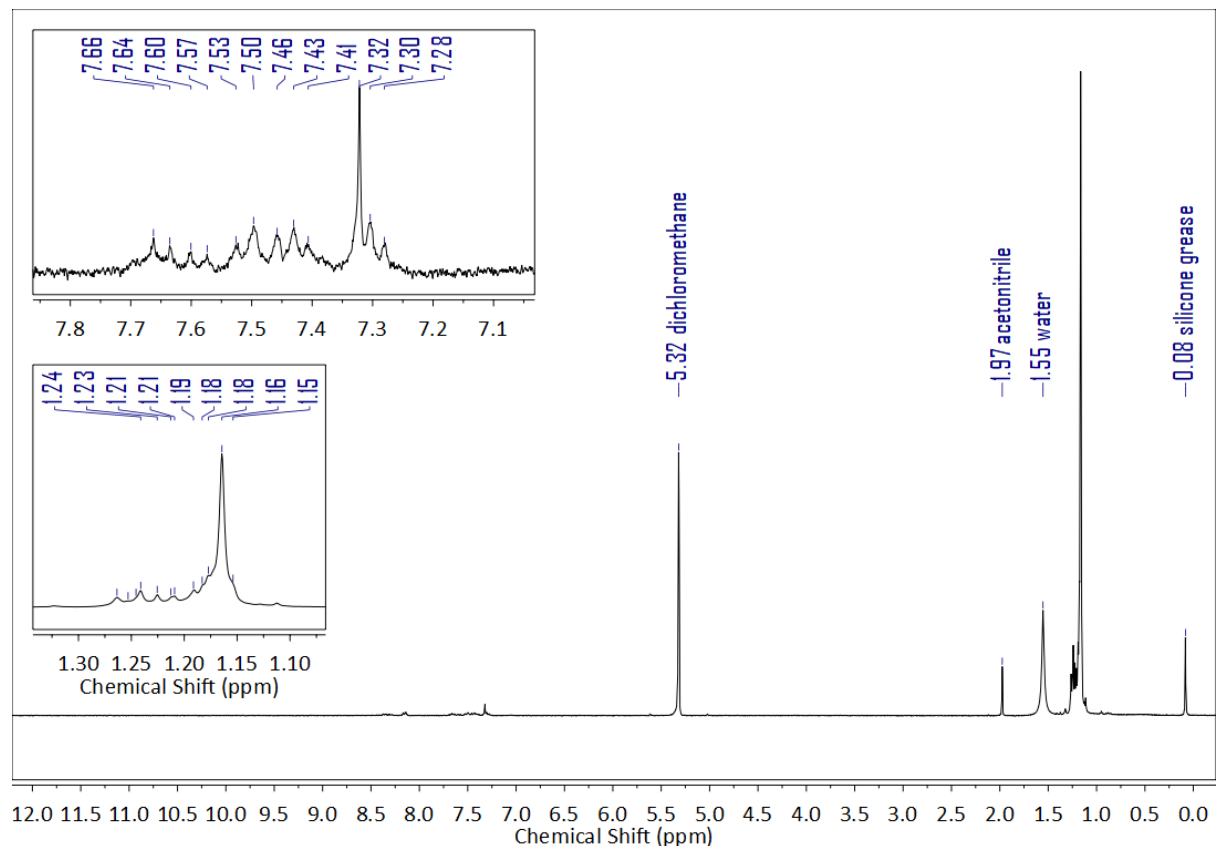


Figure S3. ^1H NMR spectrum of $\text{Ti}_8\text{L}_{15}\text{CB}$ in CD_2Cl_2 .

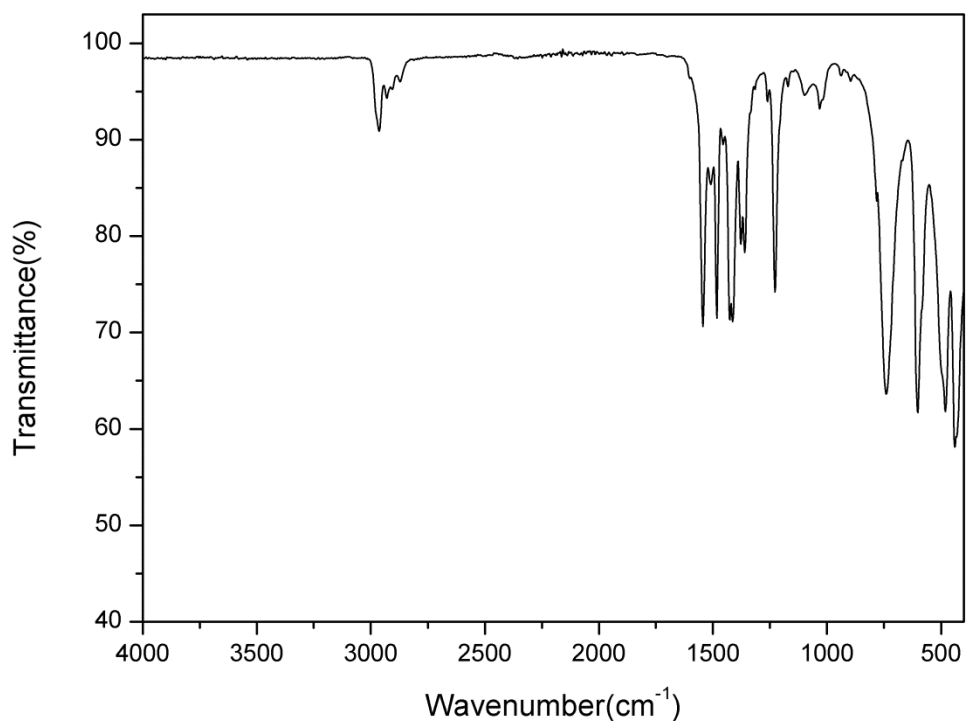


Figure S4. ATR-IR spectrum of $\text{Ti}_8\text{L}_{15}\text{CB}$.

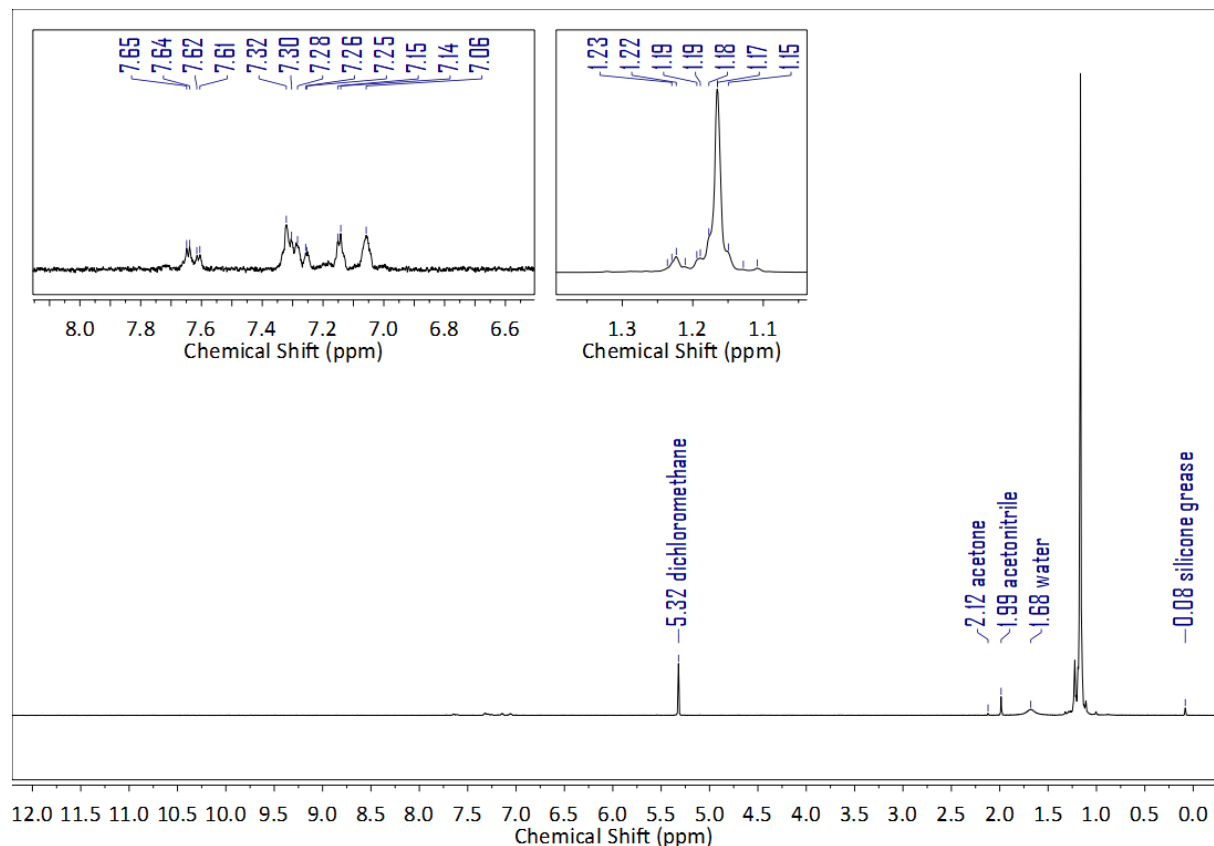


Figure S5. ^1H NMR spectrum of $\text{Ti}_8\text{L}_{15}\text{BTC}$ in CD_2Cl_2 .

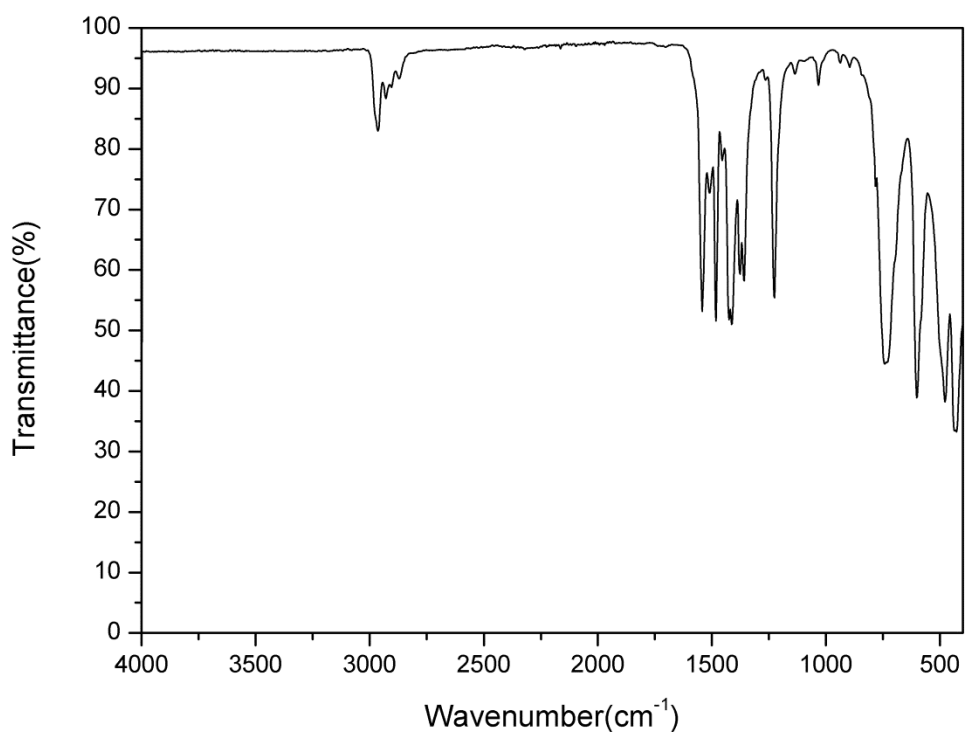


Figure S6. ATR-IR spectrum of $\text{Ti}_8\text{L}_{15}\text{BTC}$.

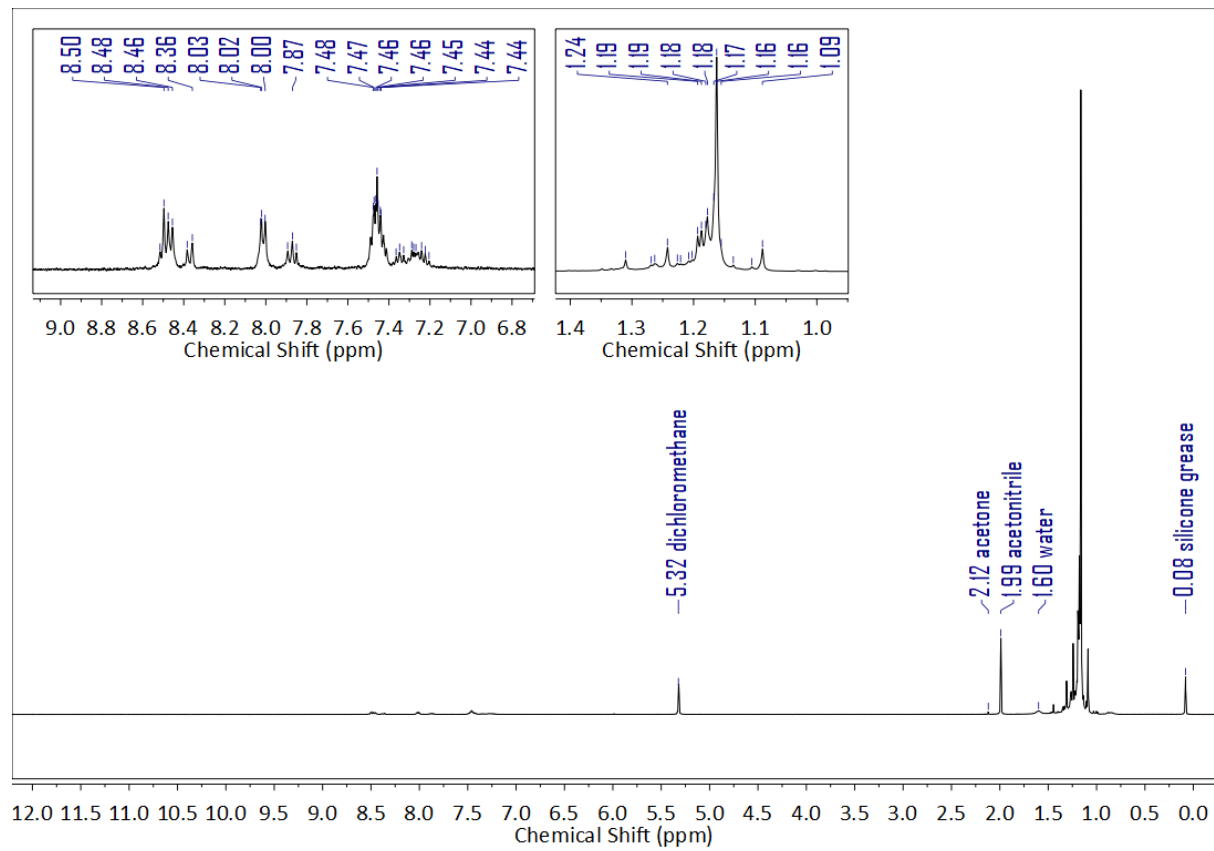


Figure S7. ^1H NMR spectrum of $\text{Ti}_8\text{L}_{15}\text{AC}$ in CD_2Cl_2 .

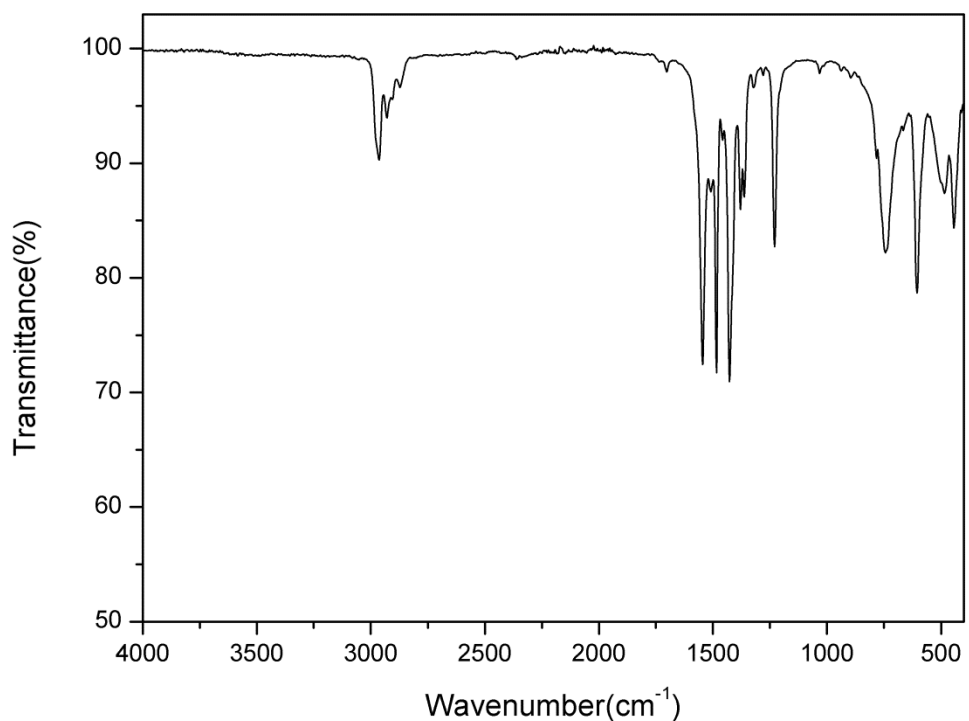


Figure S8. ATR-IR spectrum of $\text{Ti}_8\text{L}_{15}\text{AC}$.

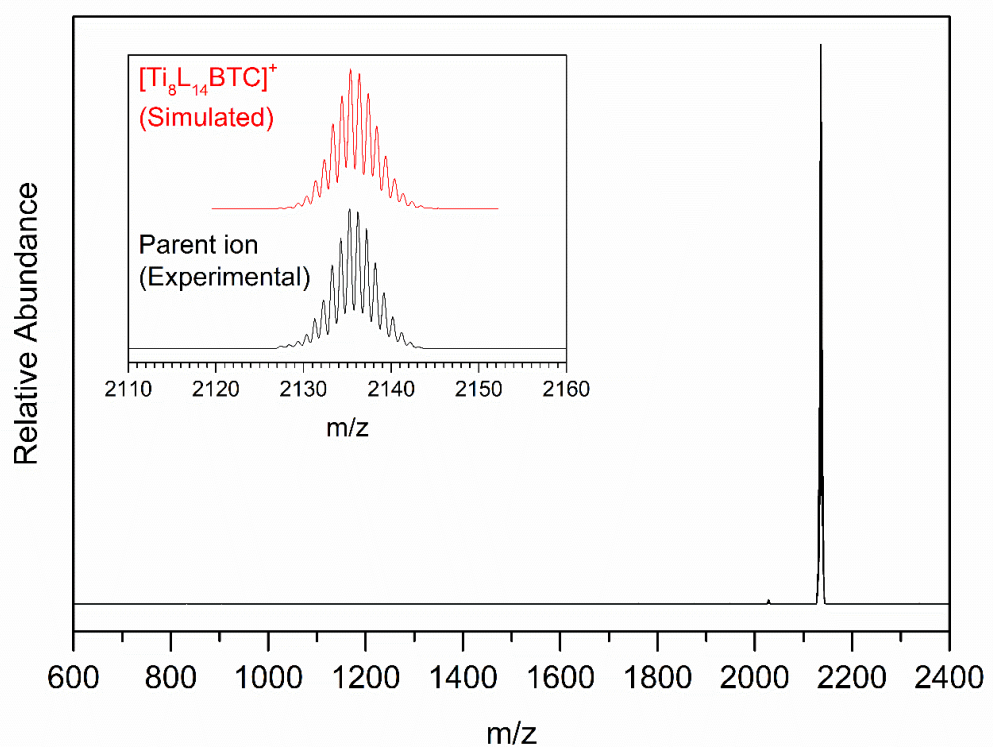


Figure S9. Mass spectrum of $[\text{Ti}_8\text{L}_{14}\text{BTC}]^+$ and simulated isotopic distribution.

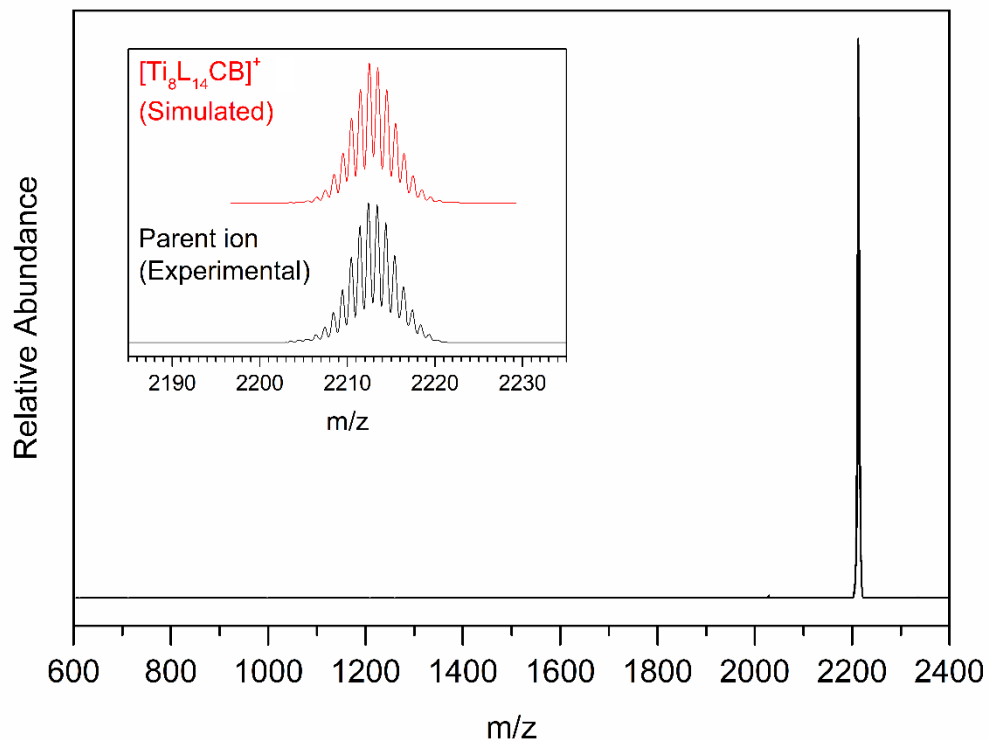


Figure S10. Mass spectrum of $[\text{Ti}_8\text{L}_{14}\text{CB}]^+$ and simulated isotopic distribution.

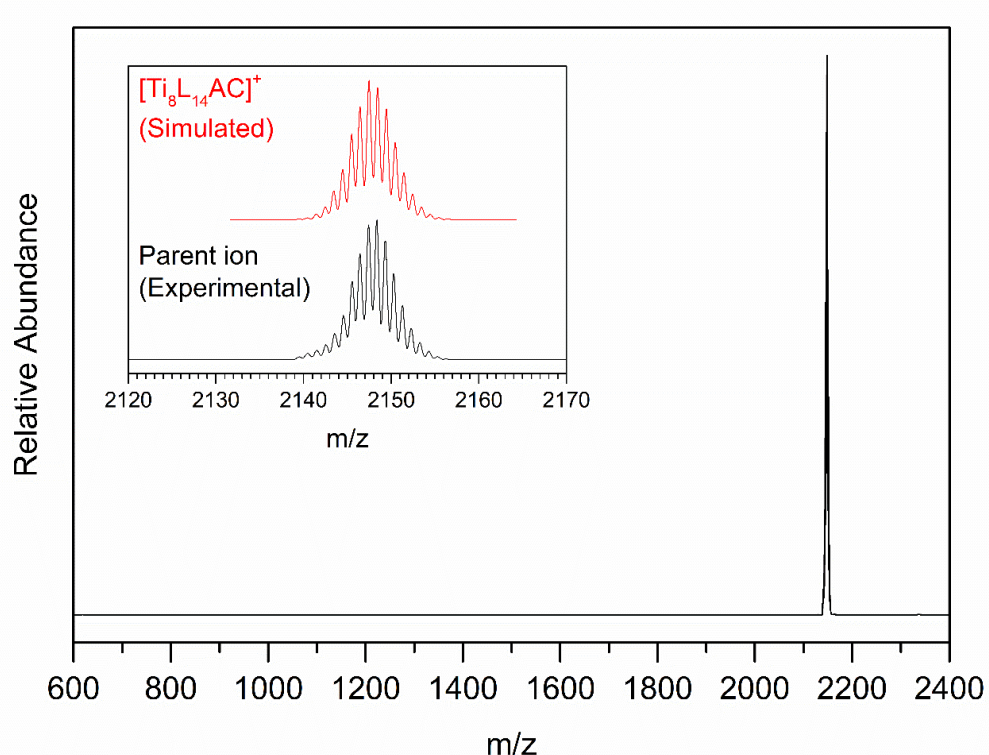


Figure S11. Mass spectrum of $[\text{Ti}_8\text{L}_{14}\text{AC}]^+$ and simulated isotopic distribution.

In the experiment, the irradiation time was controlled to keep the main product below 10% to prevent the second photon reacting with the product.

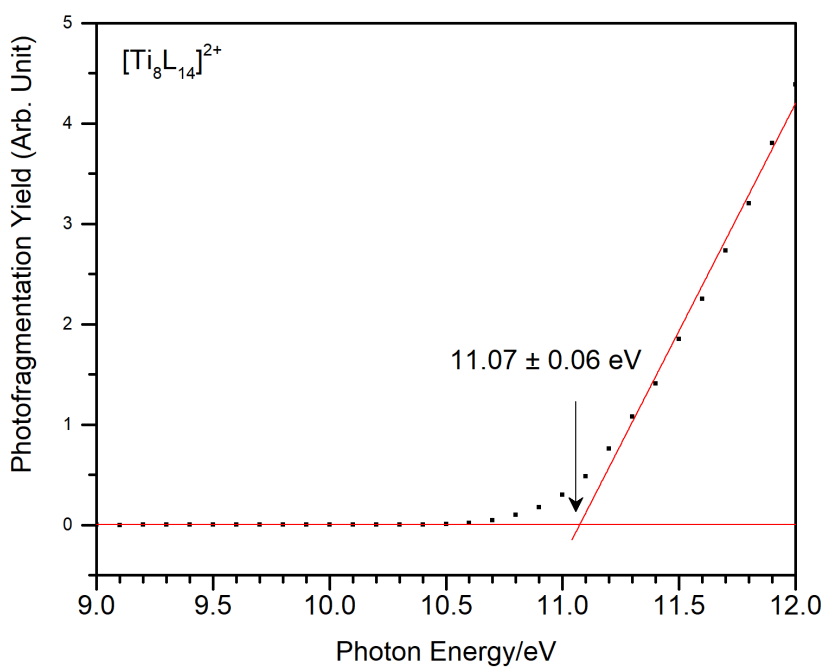


Figure S12. VUV action spectrum of $[\text{Ti}_8\text{L}_{14}]^{2+}$ and onset energy fitting.

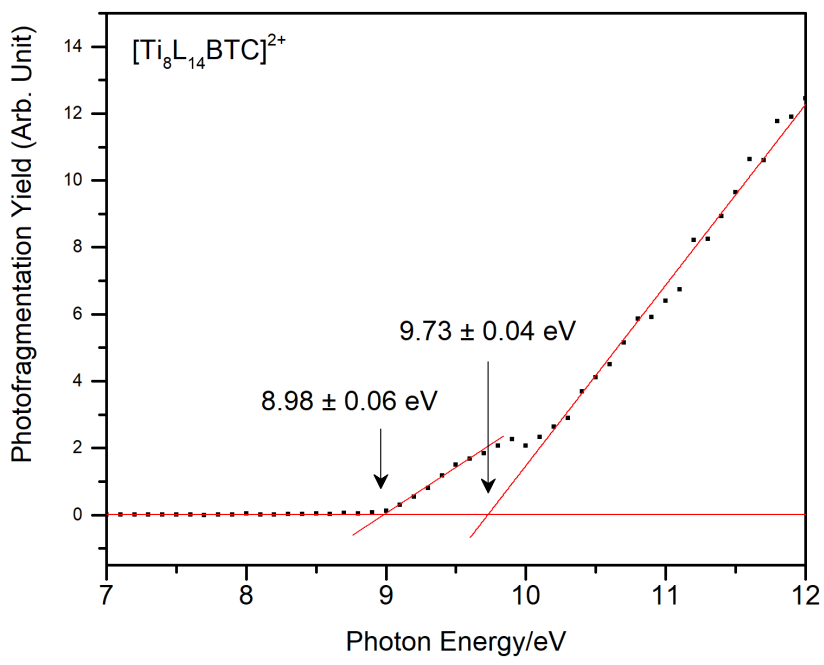


Figure S13. VUV action spectrum of $[\text{Ti}_8\text{L}_{14}\text{BTC}]^{2+}$ and onset energy fitting.

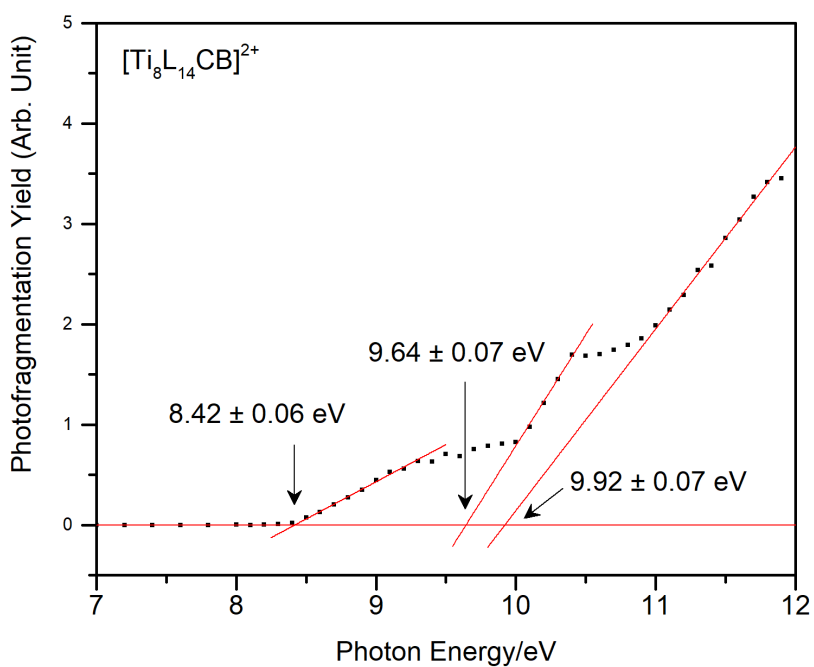


Figure S14. VUV action spectrum of $[\text{Ti}_8\text{L}_{14}\text{CB}]^{2+}$ and onset energy fitting.

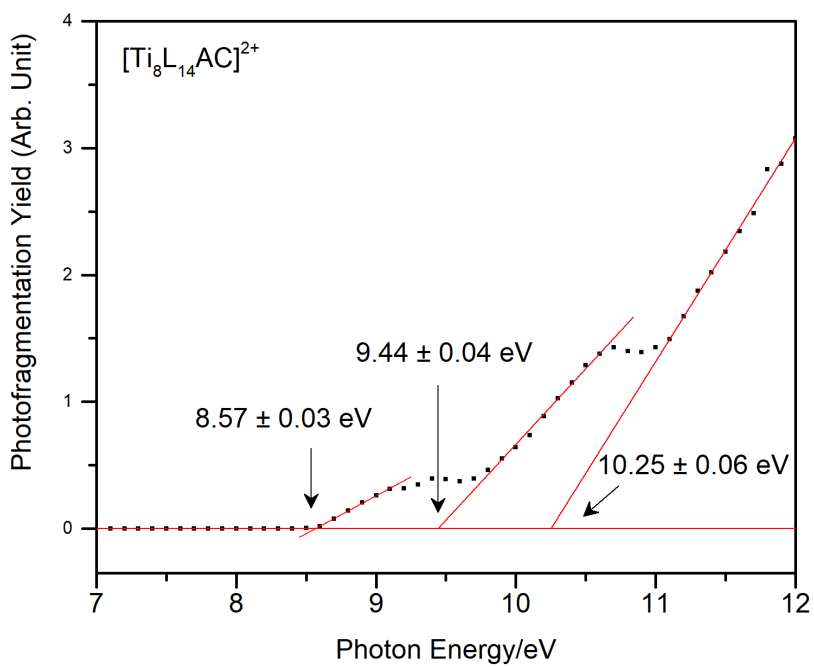


Figure S15. VUV action spectrum of $[\text{Ti}_8\text{L}_{14}\text{AC}]^{2+}$ and onset energy fitting.

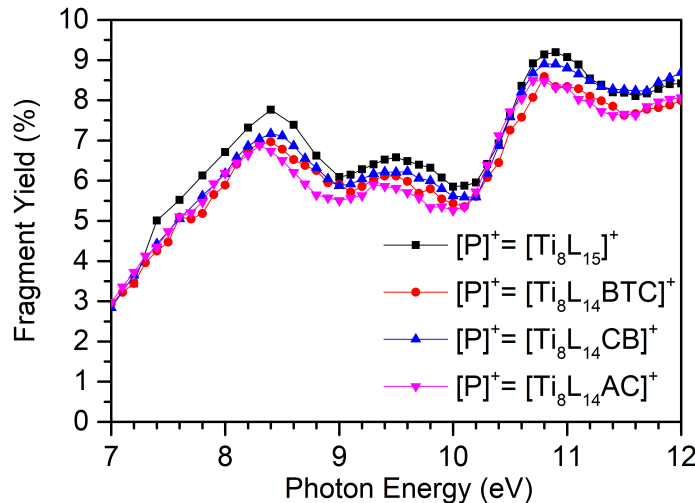


Figure S16. Fragment yield of the product resulting from pivalate photodissociation $[P-L]^+$ as a function of photon energy.

Error analysis in fragment yield calculation

The spectral dependencies, S , of each fragment are calculated as:

$$S = \frac{F}{TIC} \frac{1}{\phi} \frac{1}{t} = \frac{G}{\phi t}$$

where F is the abundance of a specific fragment, TIC the total ion current (sum of all fragments and parent ion), ϕ is the photon flux and t the irradiation time.

The error for the spectral dependencies is thus calculated as:

$$\begin{aligned} dS &= \left| \frac{1}{\partial G} \left(\frac{G}{\phi t} \right) \right| \Delta G + \left| \frac{1}{\partial \phi} \left(\frac{G}{\phi t} \right) \right| \Delta \phi + \left| \frac{1}{\partial t} \left(\frac{G}{\phi t} \right) \right| \Delta t \\ dS &= \frac{\Delta G}{\phi t} + \frac{G \Delta \phi}{\phi^2 t} + \frac{G \Delta t}{\phi t^2} \end{aligned}$$

from which the relative error is calculated as:

$$\frac{\Delta S}{S} = \frac{\left(\frac{\Delta G}{\phi t} + \frac{G \Delta \phi}{\phi^2 t} + \frac{G \Delta t}{\phi t^2} \right)}{\frac{G}{\phi t}} = \frac{\Delta G}{G} + \frac{\Delta \phi}{\phi} + \frac{\Delta t}{t}$$

The uncertainties related to the ion abundance in the mass spectrum after photon absorption (F , P , TIC and G) arise from the peak area calculation considering the uncertainty in the current detection $\Delta I = \sqrt{I}$

The maximal estimated uncertainties for photon flux and irradiation time are:

$$\frac{\Delta\phi}{\phi} = 0.1; \quad \frac{\Delta t}{t} = 0.05$$

Table S1: Summary of DFT calculation at B3LYP/6-31G(d).

MOC	E _{HOMO} (eV)	E _{LUMO} (eV)	ΔE(eV)
Ti ₈ L ₁₆ (L=acetate)	-7.365	-2.667	4.698
Ti ₈ L ₁₅ BTC (ax)	-5.859	-2.668	3.191
Ti ₈ L ₁₅ BTC (eq)	-5.658	-2.662	2.996
Ti ₈ L ₁₅ CB (ax)	-5.509	-2.695	2.814
Ti ₈ L ₁₅ CB (eq)	-5.374	-2.707	2.667
Ti ₈ L ₁₅ AC (ax)	-5.337	-2.669	2.668
Ti ₈ L ₁₅ AC (eq)	-5.143	-2.692	2.451

Complete reference to Gaussian 09

M.J. Frisch, G. W. Trucks, H. B. Schlegel, G. E. Scuseria, M. A. Robb, J. R. Cheeseman, G. Scalmani, V. Barone, G. A. Petersson, H. Nakatsuji, X. Li, M. Caricato, A. Marenich, J. Bloino, B. G. Janesko, R. Gomperts, B. Mennucci, H. P. Hratchian, J. V. Ortiz, A. F. Izmalov, J. L. Sonnenberg, D. Williams-Young, F. Ding, F. Lipparini, F. Egidi, J. Goings, B. Peng, A. Petrone, T. Hendersoon, D. Ranasinghe, V. G. Zakrzewski, J. Gao, N. Rega, G. Zheng, W. Liang, M. Hada, M. Ehara, K. Toyota, R. Fukuda, J. Hasegawa, M. Ishida, T. Nakajima, Y. Honda, O. Kitao, H. Nakai, T. Vreven, K. Throssell, J. A. Montgomery, J. J. E. Peralta, F. Ogliaro, M. Bearpark, J. J. Heyd, E. Brothers, K. N. Kudin, V. N. Staroverov, T. Keith, J. Kobayashi, K. Raghavachari, A. Rendell, J. C. Burant, S. S. Iyengar, J. Tomasi, M. Cossi, J. M. Millam, M. Klene, C. Adamo, R. Cammi, J. W. Ochterski, R. L. Martin, K. Morokuma, O. Farkas, J. B. Foresman and D. J. Fox, 2016, Gaussian, Inc., Wallingford CT